HIGH-TEMPERATURE DEFORMATION OF PRECURSOR-DERIVED MATERIALS

Günter Thurn, Martin Christ, Jerome Canel and Fritz Aldinger

Max-Planck-Institut für Metallforschung
and
Institut für Nichtmetallische Anorganische Materialien, Universität Stuttgart
Pulvermetallurgisches Laboratorium, Heisenbergstraße 5, 70569 Stuttgart, Germany
e-mail: thurn@aldix.mpi-stuttgart.mpg.de

ABSTRACT

The high-temperature deformation behavior of amorphous Si-C-N and Si-B-C-N precursor-derived ceramics was characterized by compression creep tests in a temperature range between 1200 °C and 1550 °C. The deformation consists of a stress-dependent component proportional to the applied stress and stress-independent shrinkage. The deformation can be described as viscous flow. A deformation mechanism model, developed for metallic glasses is applied on the ceramic materials. It can be shown that the time and temperature dependence of the viscosity is in good accordance with the predictions of such model.

1.INTRODUCTION

The high temperature deformation behavior liquid phase sintered silicon nitride and silicon carbide materials is controlled by the intergranular glass phase which is derived from oxide-based sintering additives[1,2]. It is involved in the major deformation mechanisms like solution-reprecipitation, viscous sliding of the grain boundaries or cavity formation. The density of grain boundaries increases with decreasing grain size. If the grain size is in the nanometer range, the materials can be deformed to a very high extend and even superplastic deformation can be observed[3]. The ultimate limit for grain size refinement is the amorphous state of a solid. Therefore the investigation of the deformation behavior of amorphous silicon nitride and silicon carbide materials is of great scientific interest. The thermolysis of organometallic polymers offers a new processing route to obtain amorphous Si-C-N and Si-B-C-N ceramics. Recent studies of the high temperature mechanical properties of as-thermolyzed Si-C-N[4,5] and Si-B-C-N materials[6,7] showed that the amorphous state of these materials reveals an outstanding mechanical stability at rather high temperatures. The deformation behavior of the amorphous precursor-derived ceramics is similar to that of metallic glasses. Therefore a deformation model developed for metallic glasses is applied to get insight into the deformation mechanisms[8,9].

2. EXPERIMENTAL PROCEDURE

Two Si-B-C-N materials derived from the T2-1[10] and MW33[11] precursors were investigated. The processing of the ceramics is described elsewhere[12]. After thermolysis in argon atmosphere at 1400 °C for 2 hours, amorphous ceramics with the chemical compositions $Si_3B_{1.0}C_{4.3}N_{2.0}$ and $Si_3B_{1.1}C_{5.3}N_{3.0}$ were obtained from the precursors T2-1 and MW33, respectively. Si-C-N materials were derived from the polyvinylsilazane (PVS) precursor (VT50, Hoechst AG, Germany) and the polyhydridomethylsilazane (PHMS) precursor (NCP200, Nichimen Corp., Japan). These materials were thermolyzed at 1050 °C and had the chemical compositions $SiC_{1.6}N_{1.3}$ and $SiC_{0.6}N$, respectively. The compression creep behavior of the four different materials was investigated in the temperature range between 1200 °C and 1550 °C in air for up to 1100 hours. The applied stresses were between 5 MPa and 300 MPa.

3. RESULTS

Figure 1 shows creep curves of the PVS-derived material tested under 100 MPa compression stress at 1400°C, 1500°C, and 1550°C. The strain rates decrease with time in very much the same way. Even after $4 \cdot 10^6$ s creep deformation at 1400°C, stationary creep is not observed. The creep results of the PHMS-derived material at a compression stress of 100 MPa are shown for different temperatures in Fig. 2. The stress dependence of the strain rates can be obtained from the curves in Fig. 3. The Si-B-C-N materials show a very similar deformation behavior. Figure 4 shows the strain rates of T2-1 and MW33 derived materials vs. time in double logarithmic scale. Obviously, the evolution of strain rate with time is the same for all the four precursor-derived materials. Therefore the deformation behavior is analyzed in detail only for the T2-1 derived material as a representative of the precursor-derived materials.

For the analysis of the creep results the Norton power-law relation

$$\dot{\varepsilon} = A \cdot t^{-c} \cdot \sigma^{n} \cdot \exp\left(\frac{-Q}{R \cdot T}\right) \tag{1}$$

was taken, where A is a constant, t the time, c the time exponent, σ is the creep stress, n the stress exponent, Q the activation energy, R the gas constant, and T the temperature in K. The time exponent of the T2-1 derived material increases from $c \approx 0.66$ (Range I) in the time range below 10^5 s to $c \approx 1$ (Range II) for times greater than ca $2 \cdot 10^5$ s. The development of the deformation rate is not dependent on the applied stress (Fig. 3 and Fig. 5). Such a behavior is fulfilled by the following relationship:

$$\dot{\varepsilon}(\sigma,t) = g(\sigma) \cdot f(t) \tag{2}$$

The influence of the temperature on the deformation rate is shown in Fig. 6. All curves show an increase in the apparent time exponent, but the transition to $c \approx 1$ occurs earlier at elevated temperatures. For the materials investigated here is $f(t) \propto t^{-c}$ with two different values of the apparent time exponent c in the two distinguished time ranges. To get the stress dependent function $g(\sigma)$ it is necessary to separate the time dependency and the stress dependency in (2) by dividing the deformation rate by the time dependent term $f(t)$. Plotting the normalized deformation rate versus the applied stress the function $g(\sigma)$ can be obtained (Fig. 6). The deformation with a linear stress dependence can be distinguished from shrinkage which is independent on the applied stress. Therefore the time and stress dependence of the deformation rate can be described empirically according to the following equation:

$$\dot{\varepsilon} = \left[\dot{\varepsilon}_0 + \dot{\varepsilon}_1 \cdot \left(\frac{\sigma}{\sigma_0}\right)^{n}\right] \cdot \left(\frac{t}{t_0}\right)^{-c} \tag{3}$$

where $\dot{\varepsilon}_0$ and $\dot{\varepsilon}_1$ are constants. To get dimensionless values the applied stress σ and the time t are normalized by σ_0 and t_0 respectively. In an analogous way the deformation in the Range II can be analyzed.

4. DISCUSSION

Due to the linear stress dependence of the deformation it is possible to calculate the viscosity

$$\eta = \frac{\tau}{\dot{\gamma}} = \frac{1}{3}\frac{\sigma}{\dot{\varepsilon}_{New}} \tag{4}$$

where $\dot{\varepsilon}_{New}$ is the Newtonian component of the deformation rate. Figure 8 shows the time dependence of the viscosity at a temperature of 1400 °C. The viscosity changes within 10^6 s by about two orders of magnitude. The line in Fig. 8 is least mean square error fit of the viscosity data to the function $\eta(t) = a + b \cdot t$. The viscosity increases linearly with time, which is also characteristic feature of other amorphous materials. The so called free volume model for the deformation of metallic glasses [8, 9] explains the viscous flow by the occurrence of flow defects. According to the model, atomic transport for structural rearrangement is caused by flow defects formed by fluctuations in the distribution of the free volume. These defects are also available for atomic transport during deformation. The strain rate $\dot{\varepsilon}$ is given by

$$\dot{\varepsilon} = 2c_f k_f \frac{\gamma_0 v_0}{\Omega} \sinh\left(\frac{\sigma \gamma_0 v_0}{2kT}\right) \tag{5}$$

where c_f represents the concentration of flow defects, k_f the jump frequency of a defect, γ_0 the shear strain per jump of a single defect, v_0 the volume of one defect and Ω the atomic volume. In the low stress regime, where the approximation $\sinh(\sigma\varepsilon_0 v_0/2kT) \approx \sigma\varepsilon_0 v_0/2kT$ is valid, the model predicts the Newtonian viscosity η:

$$\eta = \frac{kT\Omega}{c_f k_f (\gamma_0 v_0)^2} \tag{6}$$

The jump frequency k_f is thermally activated and can be written as

$$k_f = \upsilon_0 \exp\left(-\frac{Q}{RT}\right) \tag{7}$$

where υ_0 is expected to be about the Debye frequency and Q is an activation energy. The viscosity change with time in this model is explained by the annealing of the flow defects that results in a decrease of the amount of free volume. The defect concentration c_f varies with time and temperature [9]:

$$c_f^{-1} = c_{f_0}^{-1} + C_0 t \exp\left(-\frac{Q}{RT}\right) \tag{8}$$

In this equation, c_{f_0} represents the starting value of the defect concentration c_f and C_0 is constant. In the temperature range well below the glass transition temperature, the value of $(\gamma_0 v_0)$ is assumed to be temperature-independent. Further is assumed that the activation energy for the movement of defects (7) and the activation energy for production and annihilation of defects (8) are equal. Therefor in this temperature range the viscosity according to the free volume model can be expressed by inserting (7) and (8) in (6):

$$\eta(T,t) = \left[\frac{CT}{c_{f_0}} \exp\left(\frac{Q}{RT}\right)\right] + [CC_0 T] \cdot t \tag{9}$$

with the constant

$$C = \frac{k\Omega}{(\gamma_0 v_0)^2 \upsilon_0} \tag{10}$$

The free volume model yields a linear relation between viscosity and time in accordance with the experimental results (Fig. 8).

The time dependence of the viscosity is shown in Fig. 9 for different temperatures. The dashed line represents linear time dependence. As expected, this slope is approached asymptotically in the temperature range investigated. Whereas the viscosity varies much with temperature at low times, it seems to be rather independent of the temperature at times exceeding $3 \cdot 10^5$ s. The values of $a(T)$ were obtained by fitting a linear function to the data shown in Fig. 9. The free volume model predicts the following relation between $a(T)$ and T:

$$a(T) \propto T \exp\left(\frac{Q}{RT}\right) \tag{11}$$

As can be seen from Fig. 10 the temperature dependence of the starting viscosity is in accordance with the free volume model. From the slope of the straight line in Fig. 10 the activation energy $Q \approx 0.6$ MJ/mol for jumps and annihilation of the flow defects can be calculated.

REFERENCES

1 R. Kossowsky, D. G. Miller, and E. S. Diaz, Tensile and Creep Strength of Hot-pressed Si_3N_4, J. Mater. Sci. 10 (1975) 983-997.

2 W. E. Luecke, S. M. Wiederhorn, B. J. Hockey, R. F. Krause Jr., and G. G. Long, Cavitation Contributes Substantially to Tensile Creep in Silicon Nitride, J. Am. Ceram. Soc. 78 (1995) 2085-96.

3 F. Wakai, Y. Kodama, S. Sakaguchi, N. Murayama, K. Izaki, and K. Niihara, A Superplastic Covalent Crystal Composite, Nature 344 (1990) 421-423.

4 J. Bill and F. Aldinger, Precursor-Derived Covalent Ceramics, Advanced Materials 7 (1995) 775-787.

5 G. Thurn, J. Canel, J. Bill and F. Aldinger, Compression Creep Behavior of Precursor-Derived Si-C-N Ceramics, J. Europ. Ceram. Soc. 19 (1999) 24-30.

6 L. An, R. Riedel, C. Konetschny, H.-J. Kleebe and R. Raj, Newtonian Viscosity of Amorphous Silicon Carbonitride at High Temperature, J. Am. Ceram. Soc. 81(1998) 1349-52.

7 B. Baufeld, H. Gu, J. Bill, F. Wakai and F. Aldinger, High Temperature Deformation of Precursor-Derived Amorphous Si-B-C-N Ceramics, J. Europ. Ceram. Soc., in press.

8 F. Spaepen, in Physics of Defects, R. Balian, M: Kléman and J.-P. Poirier (eds.), Les Houches Lectures XXXV, 1980, 134-174.

9 A. van den Beukel, E. Huizer, A. L. Mulder and S. van den Zwaag, Change of Viscosity During Structural Relaxation of Amorphous $Fe_{40}Ni_{40}B_{20}$, Acta metall. 34 (1986) 483-492.

10 A. Kienzle, PhD Thesis, Universität Stuttgart 1994.

11 M. Weinmann, J. Schuhmacher, H. Kummer, S. Prinz, J. Peng, H. J. Seifert, K. Müller, J. Bill and F. Aldinger, Synthesis and Thermal Behavior of a Novel Si-B-C-N Ceramic Precursor, Chem. Mater., submitted.

12 R. Haug, M. Weinmann, J. Bill and F. Aldinger, Plastic Forming of Preceramic Polymers, J. Europ. Ceram. Soc. 19 (1999) 1-6.

Figures

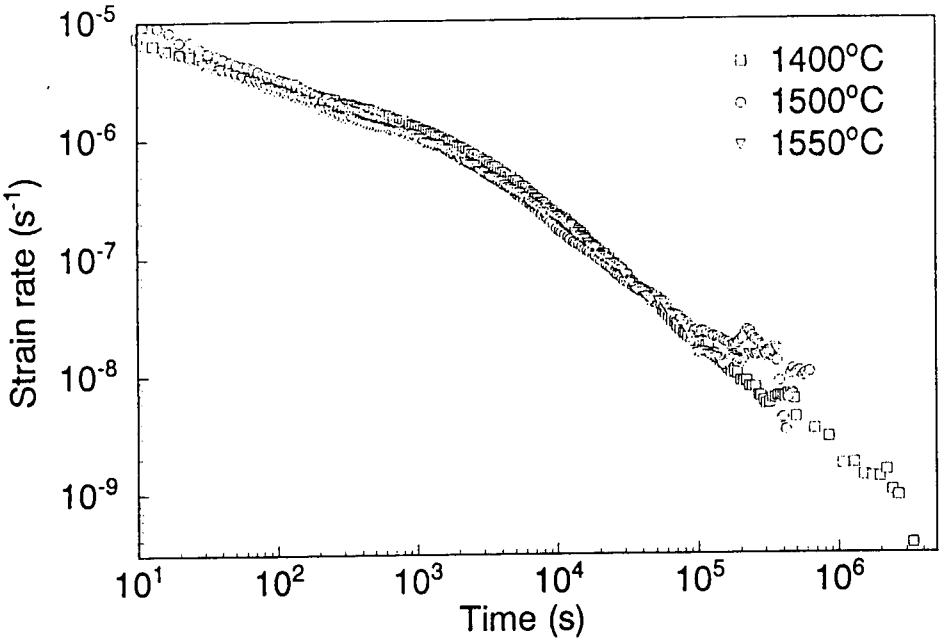

Fig. 1. Temperature dependence of the strain rates at a compression stress of 100 MPa for the PVS-derived material.

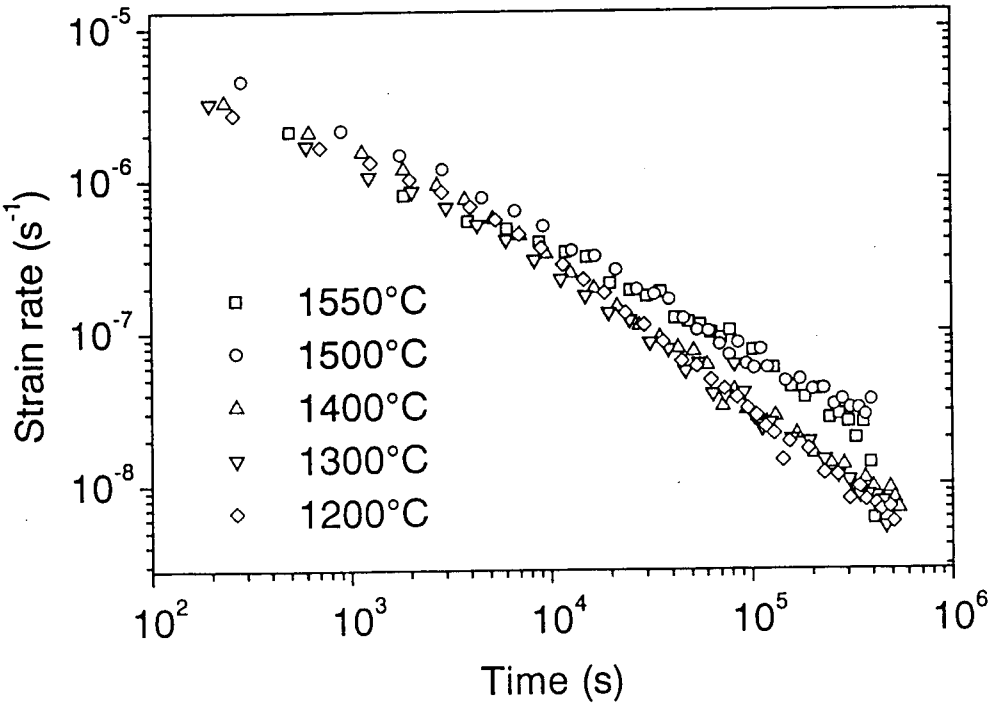

Fig. 2. Temperature dependence of the strain rates at a compression stress of 100 MPa for the PHMS-derived material.

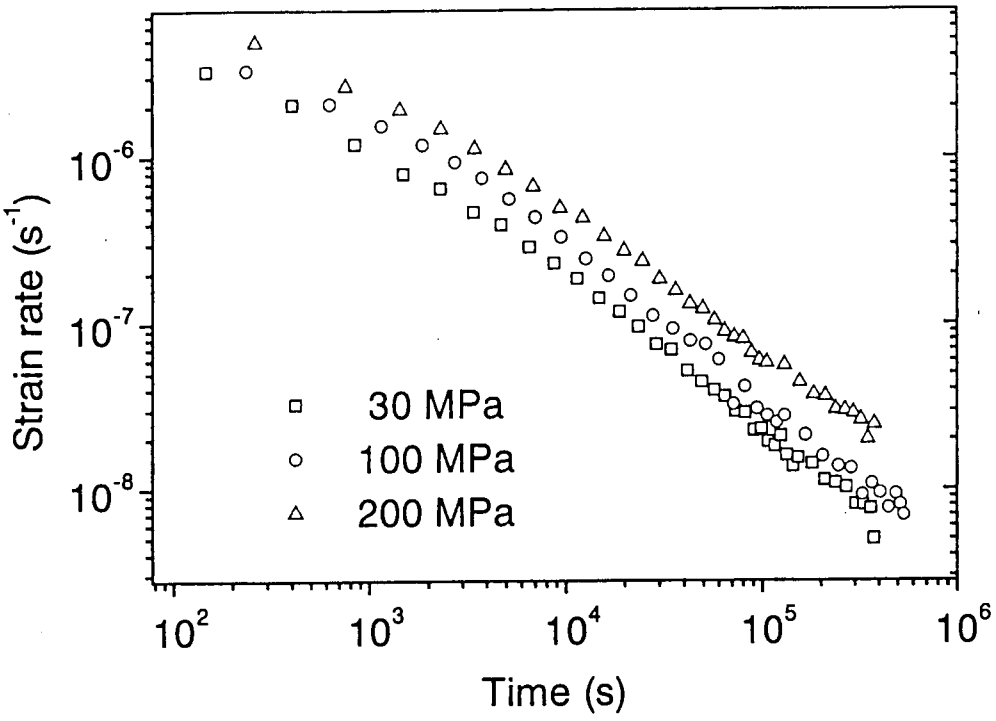

Fig. 3. Stress dependence of the strain rates at 1400 °C for the PHMS-derived material.

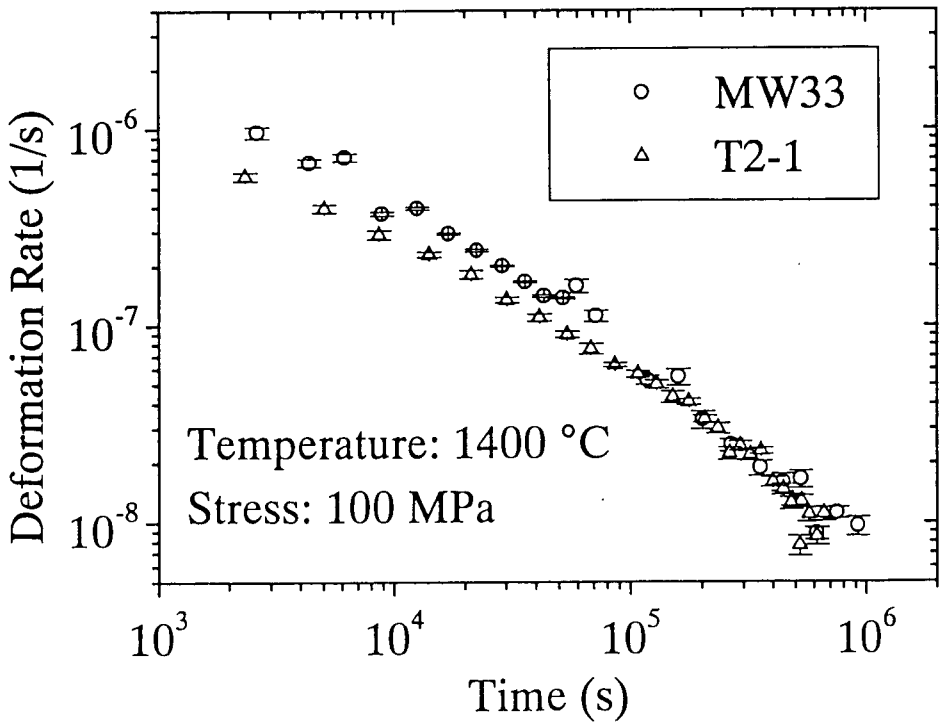

Fig. 4. Comparison of the deformation rates of MW33 and T2-1 derived amorphous ceramics during isothermal creep tests

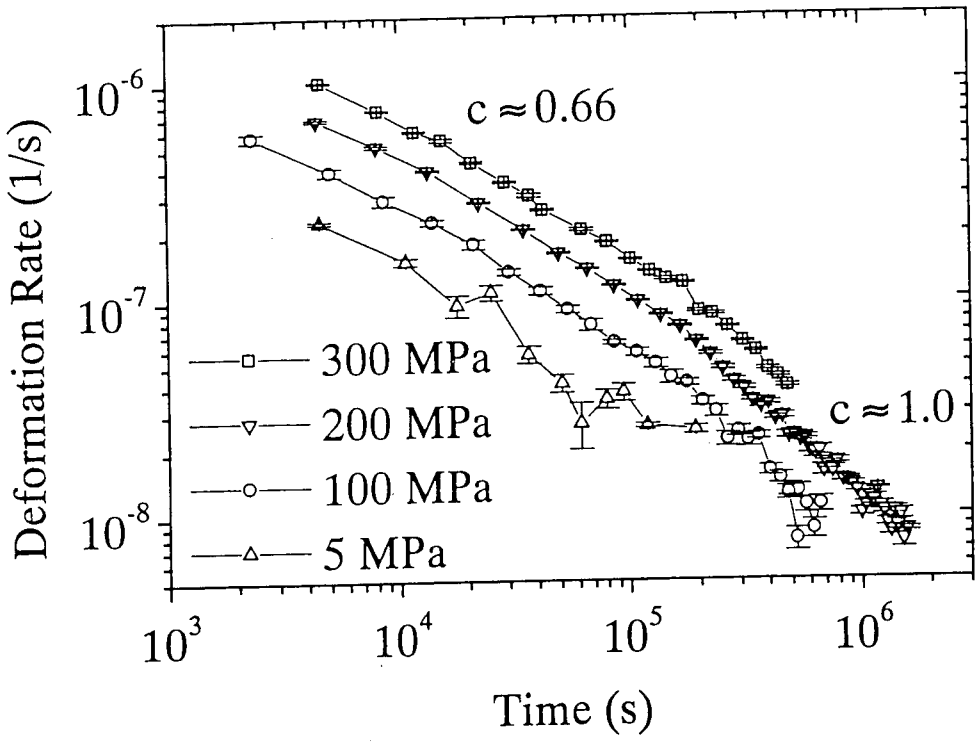

Fig. 5. Creep rates vs. time for different applied compressive stresses. The tests were performed with T2-1 derived ceramics at 1400 °C.

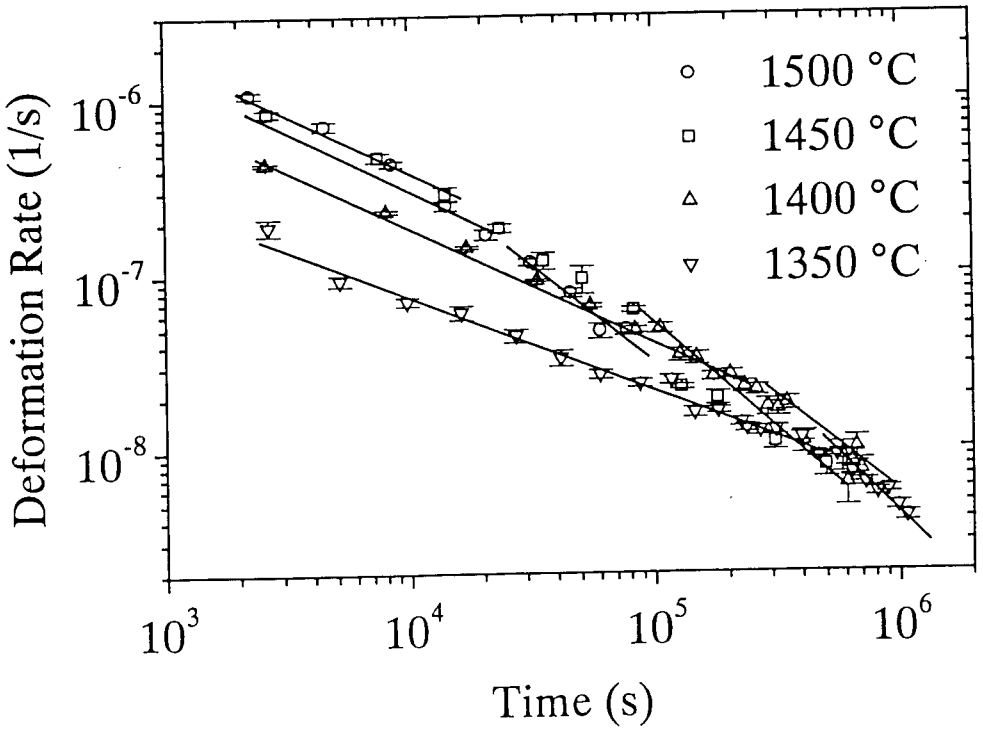

Fig. 6. Creep rates vs. time for different temperatures temperature. The tests were performed with T2-1 derived ceramics at 50 MPa.

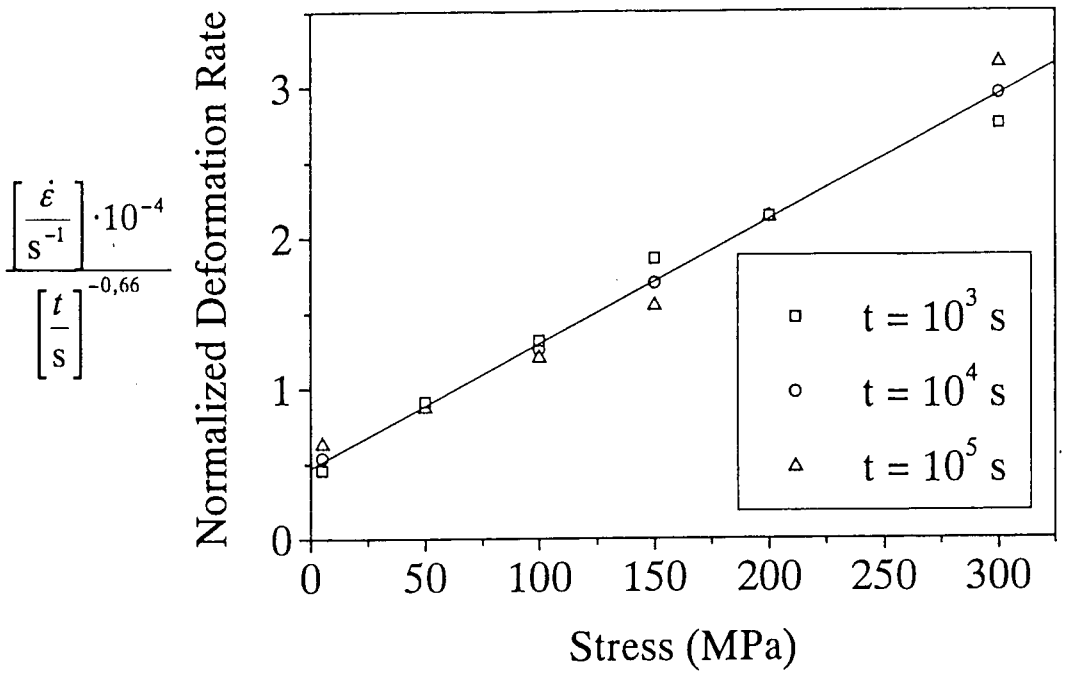

Fig. 7. Stress dependence of normalized deformation rate of T2-1 derived ceramic at 1400 °C in Range I ($t < 10^5$ s).

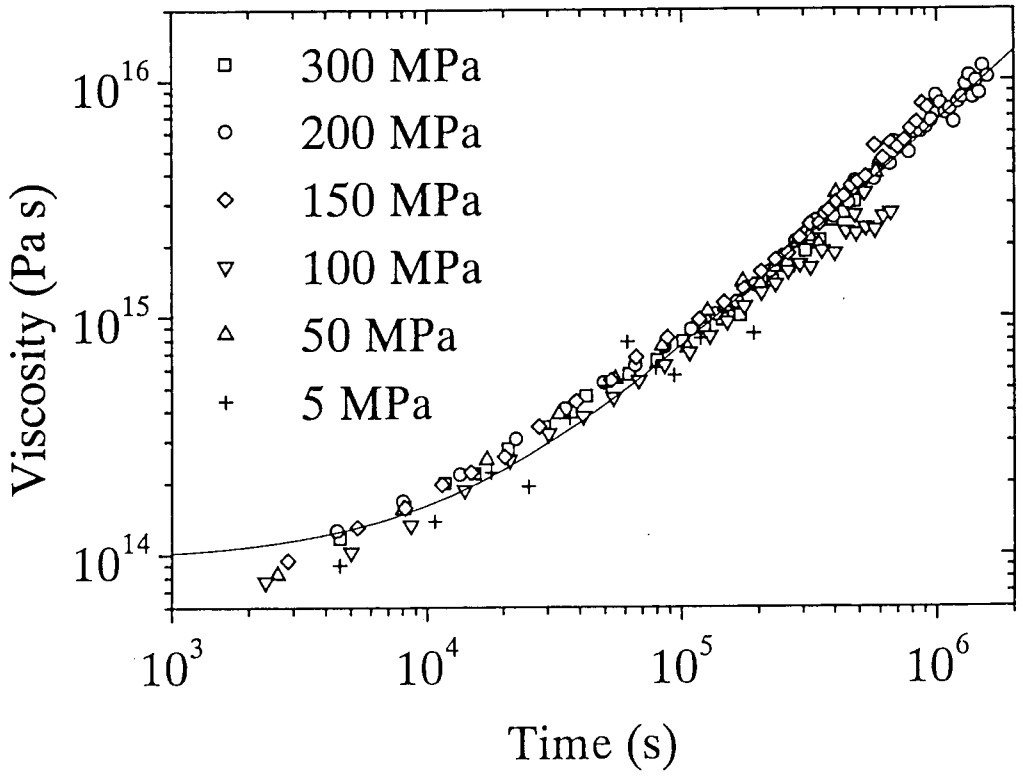

Fig. 8. Measured data and fitted curve of the time dependent viscosity of T2-1 derived amorphous ceramic.

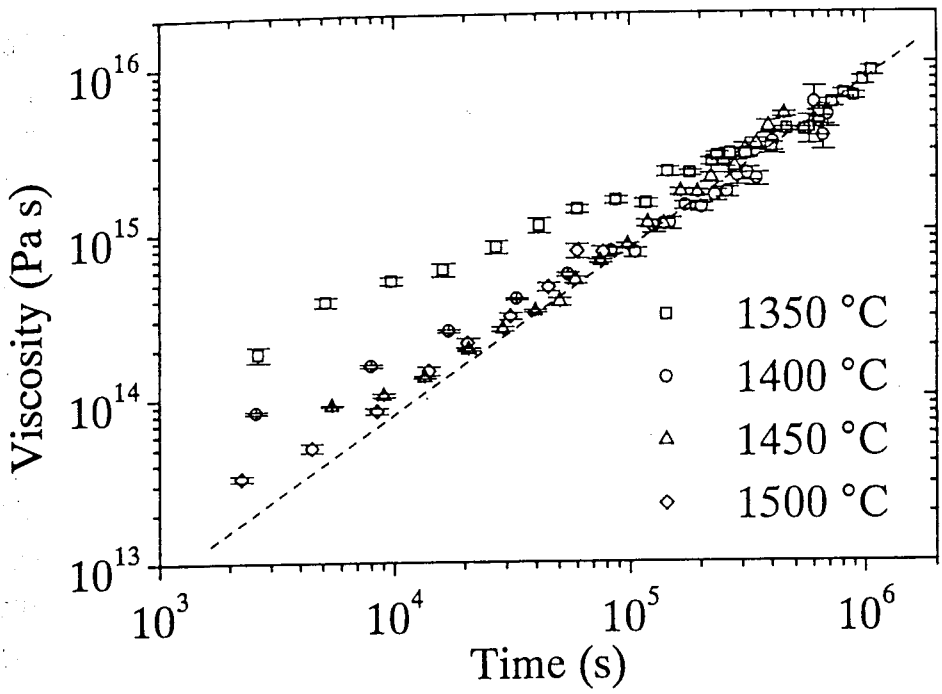

Fig. 9. Variation of the viscosity of T2-1 derived amorphous ceramic with time and temperature. All deformation tests were performed at 50 MPa.

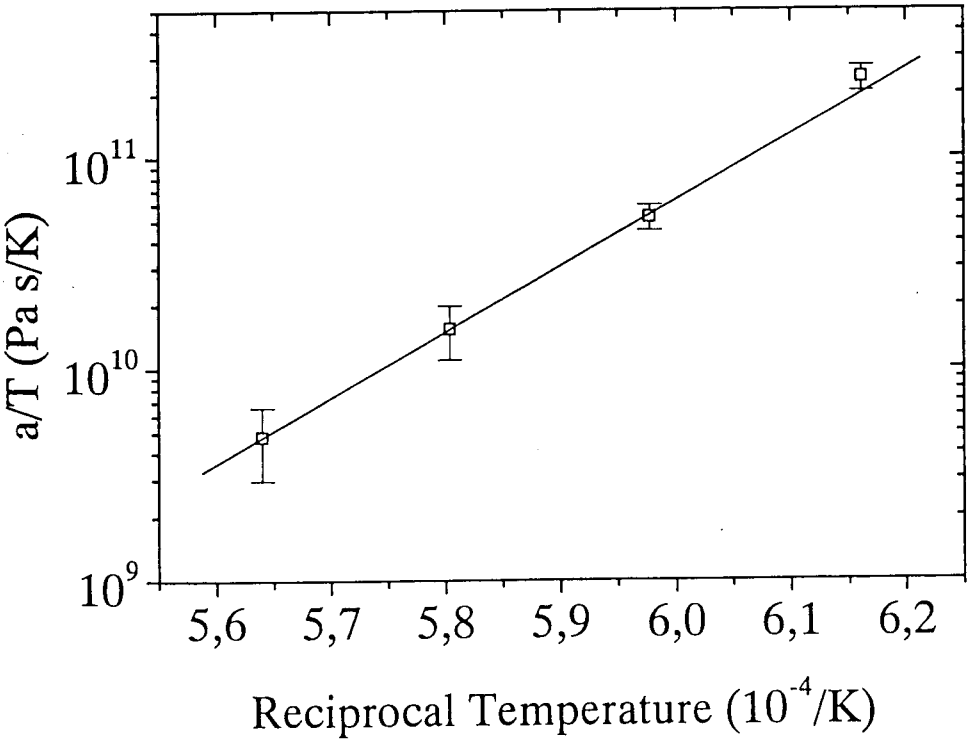

Fig. 10. Temperature dependence of the starting viscosity $a(T)$ plotted according to the free volume model. Solid line: Prediction of the model, symbols: experimental results.